Optics and Lasers in Engineering 166 (2023) 107587

Contents lists available at ScienceDirect

Optics and Lasers in Engineering

journal homepage: www.elsevier.com/locate/optlaseng

A quantitative laser speckle-based velocity prediction approach using machine learning

Xiaoqi Hao[a], Shuicai Wu[a], Lan Lin[a], Yixiong Chen[b], Stephen P. Morgan[c], Shen Sun[a,*]

[a] Faculty of Environment and Life, Beijing University of Technology, No. 100 Pingleyuan, Chaoyang District, Beijing, 10012, China
[b] Beijing Science and Technology Project Manager Management Corporation Ltd, Beijing, China
[c] Optics and Photonics Research Group, University of Nottingham, Nottingham, UK

ARTICLE INFO

Keywords:
Laser speckle contrast imaging (LSCI)
Blood flow imaging
Machine learning
Convolutional neural network (CNN)
Microcirculation

ABSTRACT

Laser speckle contrast imaging (LSCI) can be applied to non-invasive blood perfusion measurement with high resolution and fast speed. However, it is lack of measurement accuracy. The aim of this study is to enable quantitative measurement of LSCI by using Artificial Intelligence (AI), and this is achieved by using a set of experimental data obtained from a rotating diffuser (a tissue phantom mimicking blood flow under skins) within simulated flow velocity of 0.08–10.74 mm/s. These data were used to train a three-dimensional convolutional neural network (3D-CNN) to establish a LSCI velocities prediction model (CNN-LSCI) with behavioral feature learning. The trained model has 0.33 MSE (mean squared error) and 0.34 MAPE (mean absolute percentage error) and is verified by ten phantom velocities (0.2-4 mm/s, step is 0.445 mm/s) covering the typical blood flow velocity range of human body (0-2 mm/s) with the correlation of 0.98. The better performance of the proposed model is demonstrated by the results compared to traditional LSCI and multi-exposure laser speckle contrast imaging (MELSCI). This study shows the potential of LSCI to achieve quantitative blood perfusion measurement using machine learning.

1. Introduction

Blood perfusion of microcirculation on body surface is a significant indicator. It is widely used in various fields such as the microcirculatory imaging during surgery [1,2], the functional imaging of human retina [3,4], the prevention of diabetic foot ulcer [5,6], the assessment of wound healing [7,8], the animal model evaluation [9,10] and the biological experiment [11] *etc*. Laser speckle contrast blood flow imaging (LSCI) featured by noninvasive measurement, fast imaging speed and system simplicity is well developed and prevalently used to detect the flow perfusion in both clinic and research. It is based on the dynamic light scattering principle to setup different approximate models under certain assumptions, calculating the autocorrelation function of scattered light which is related to the blood flow velocity. However, because of the existence of static scatterers, mismatched speckle size, narrow range of exposure times LSCI is lack of quantitative measurement, restricting its clinical application. Consequently, it is of great interests in making it be capable to measure blood flow quantitatively.

Over the last few decades, improvements have mainly been achieved by either developing more robust LSCI calculation models [12–17] or applying multiple exposure times [18–20]. The improved LSCI models take account the effects of static scattering [12,13], mismatched speckle size [14,15], noise caused by non-ergodic light [16,17]. However, measurement accuracy is still affected by the uncertainties introduced by the assumptions when setting up the speckle model, nonpredictable complex light transmission path and imaging system noise. The multiple-exposure laser speckle contrast imaging (MELSCI) alternatively obtains the blood perfusion by fitting a series of contrast at different exposure times. As a result, linearity has been enhanced by eliminating the dependence of exposure time. While the process of fitting calculation requires longer time [18], resulting in lower temporal resolution. In addition, MELSCI is hard to perform real-time blood flow imaging because the fitting process is typically operated offline. Consequently, the mainstream commercial LSCI instruments are still developed based on the single exposure model.

In recent years, Artificial Intelligence (AI) has been introduced to improve LSCI measurement. K-means clustering [21], as a typical machine learning method, is applied to the calculation of LSCI contrast for determining the localization of blood vessels. It helps with locating blood vessels, but it is only applicable when the blood vessels and tissue regions are well separated from each other. Cheng et al. applied a feed-forward denoising convolutional neural network (DnCNN) to LSCI [22]. In operation, the training was carried out in the log-transformed domain. As a result, the inhomogeneous noise distribution is effectively removed.

* Corresponding author.
E-mail address: sunshen@bjut.edu.cn (S. Sun).

https://doi.org/10.1016/j.optlaseng.2023.107587
Received 31 December 2022; Received in revised form 10 March 2023; Accepted 17 March 2023
Available online 24 March 2023

The superior performance of using DnCNN has been demonstrated by 5.13 dB improvement of the peak signal-to-noise ratio (PSNR). Stebakov et al. trained a feed-forward ANN to predict the flow rate in glass capillaries (0-2 mm/s) by classification recognition [23]. Although improvement of prediction accuracy has been demonstrated, the classification only covered a few discrete flow rates. Kornaeva et al. combined LSCI with deep learning to propose a method for measuring viscosity of non-Newtonian fluids [24]. A Resnet18 network model was trained using LSCI images of inertial flow in a torus-shaped capillary. This model could predict the shear rate on the inner surface of the capillary and the flow rate from speckle images of experimental fluids. A modified mathematical model was used to calculate the viscosity of non-Newtonian fluids. This work demonstrated the outstanding performance of applying deep learning to LSCI as the relative error is less than 2% for the tested non-Newtonian fluid and less than 0.5% for the tested Newtonian fluid. This makes it possible to use the viscometer as a testing device in medicine fluid, especially the rheology of blood. Fredrekson *et al.* demonstrated that multi-exposure LSCI can perform LDI-like measurement by utilizing machine learning [25]. In that study, an ANN model was trained with Monte Carlo simulated data. The results showed high accuracy with correlation coefficient $R = 1.000$ for noise-free data and $R = 0.993$ for noisy data. This ANN model was also evaluated in post congestion experiment with high accuracy of $R = 0.995$. This study demonstrates the feasibility of using ANN to calibrate LSCI to LDI and illustrates the great flexibility of machine learning applied to LSCI. However, as the LDI data is system dependent, the accuracy of the ANN model will vary with the front-end bandwidth, system noise and optical settings. The above researches demonstrate the high potential of utilizing machine learning in LSCI. This is because the 'black box' eliminates the influence of uncertain factors in comparison to the traditional speckle-based methodologies.

In this paper, a velocity prediction model is established by using machine learning. A state-of-art deep learning architecture, 3D-CNN (Three-Dimensional Convolutional Neural Network), is adopted to set up the model mapping LSCI speckle images to flow velocity distributions. To achieve quantitative measurement, a set of well-controlled experimental data was generated by mimicking RBCs (Red Blood Cells) flowing under superficial tissues with known velocity distributions. This method is evaluated by comparing with traditional LSCI and MELSCI with same data.

This paper is organized as below. Following the introduction in Section 1, the used experimental data and the basic theory of spatio-temporal speckle is elaborated in Section 2. Section 3 details the setup of the 3D-CNN model in terms of structures, training process and evaluations. In Section 4, the results are displayed and compared to both traditional LSCI and MELSCI. This paper is ended with the conclusion and discussion presented in Section 5.

2. Material and methods

2.1. The database

In this paper, the model is constructed by using the experimental data of rotating scattering plate (the phantom). The schematic diagram of the rotating scattering plate is shown in Fig. 1, which is composed of a servo motor, a uniform diffuse reflection plate and a frosted glass reflector. During the experiment, the motor drives the animation reflector to rotate behind the ground glass at a certain angular speed, simulating the flow of red blood cells in human tissue under the epidermis.

The experimental setup is shown in Fig. 2. A green laser beam (OXXIUS S.A. 532 S-50-COL-PP, 532 nm, 50 mW) is expanded to a diameter of 18 mm by a diffuser (BE20, Thorlabs) and reflected onto the static diffuser with a diameter of 20 mm. The white cardboard disc (diameter 30 nm) rotates at a controlled velocity. The lens (Sechneider, $f = 12$ mm) is placed 72 mm away from the diffuser and forms an image on the CMOS sensor with a magnification of 0.2. In addition, the f number of the lens' aperture is adjusted to 13 to set the speckle diameter twice the pixel width [26].

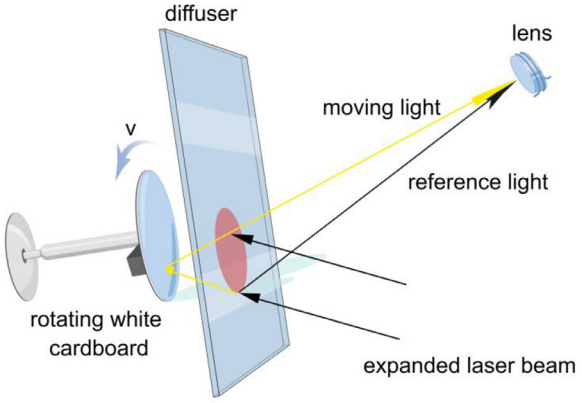

Fig. 1. Schematic diagram of rotating scattering plate phantom [26].

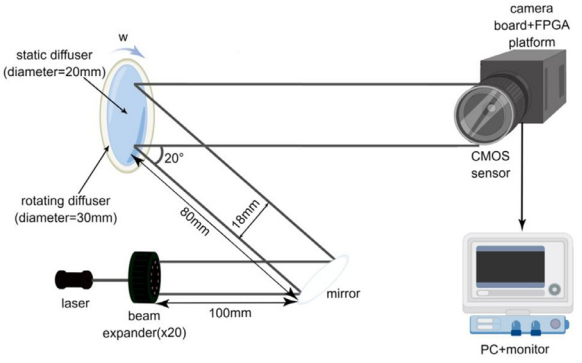

Fig. 2. Experiment setup of rotating scattering plate phantom [26].

The LSCI system used in this experiment consists of imaging unit, memory unit and processing unit. The imaging unit uses a megapixel CMOS image sensor (MT9M413) with controllable region of interest (ROI). It contains 1280 × 1024 integrating pixels, 1280 column-parallel 10-bit ADCs and ten 10-bit-wide digital output ports that provide fast data transmission. The memory unit uses DDR3 SDRAM (double data rate type three synchronous dynamic random-access memory) featured by high bandwidth and huge capacity. Depending on the clock rate, it can transfer data at a rate of 800–2133 MT/s (megatransfers per second), which can satisfy the large-memory required for high-resolution images and the bandwidth required for high frame rate. A FPGA platform (Virtex 6 XC6VLXC240T) is adopted to interface to the FPGA. The raw data was transformed and pre-processed in this FPGA platform.

In experiment, the imaging system is operated at fixed exposure time of 10.4 ms. The motor controls diffuser rotating from 0.047 rad/s up to 0.952 rad/s with a fixed incremental step of 0.106 rad/s, as shown in Table 1. 1024 frames were captured around every 10 s at each measurement, equivalenting to ~100 FPS (frame per second). At each angular velocity, 32 × 320 is intercepted as the size of each data, as shown in Fig. 3(a). So, the size of the speckle dynamic map measured each time is 32 × 320 × 1024 (the image resolution is 32 × 320, with 1024 frames).

The advantage of using this experimental data is that it enables quantitative evaluations as all velocities are known and under control during experiment. Besides, the speckle data obtained in the experiment contains the instrument noise and optical noise which are crucial for training the 3D-CNN model.

Table 1
angular velocity.

Number	1	2	3	4	5	6	7	8	9	10
Angular speed (rad/s)	0.047	0.105	0.210	0.317	0.424	0.530	0.636	0.741	0.848	0.952

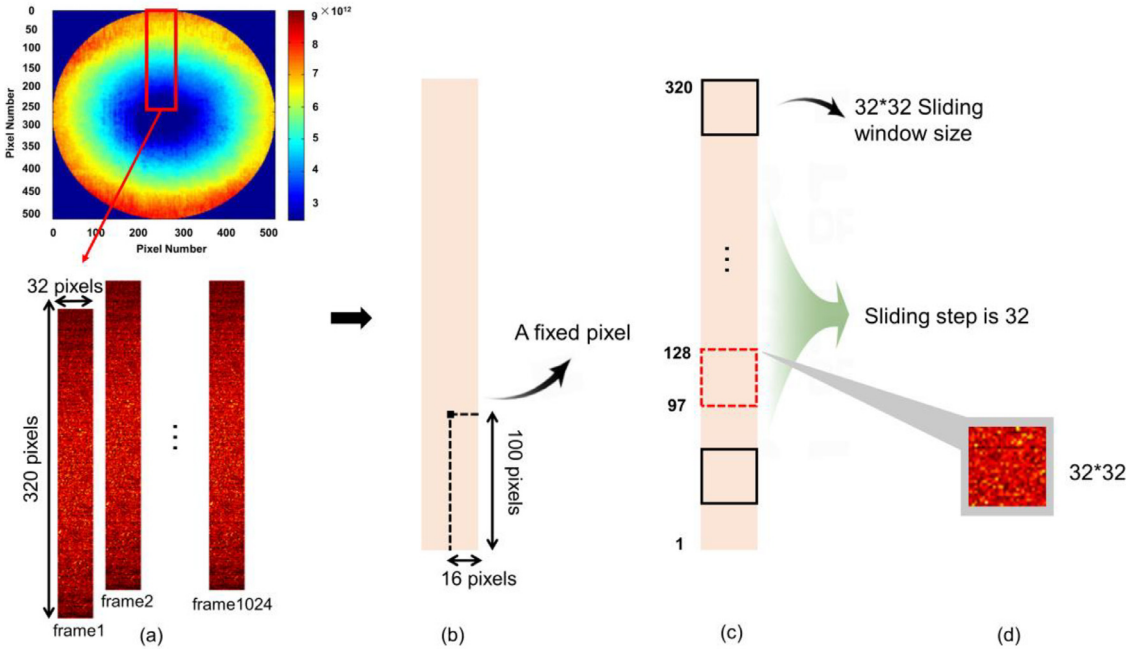

Fig. 3. Speckle data and process. LSCI dynamic map of phantom of rotating scattering plate is shown in (a), the selection of a fixed pixel for feature analysis is shown in (b), radius selection method is shown in (c), the selection of test data is shown in (d).

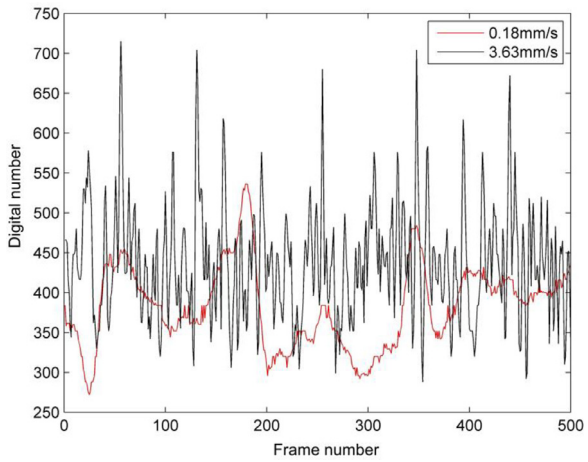

Fig. 4. Pixel value changes of two velocities at (16,100) point with 500 frames.

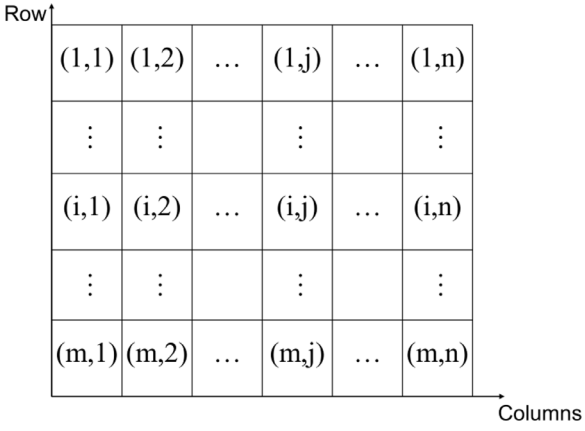

Fig. 5. pixel position distribution of speckle single frame image.

2.2. Analysis of spatio-temporal features

In the speckle dynamic map of LSCI, the pixel values of a single frame speckle image contain rich spatial information, and the changing rule of the pixel value at a fixed position with time is closely related to the velocity. This means velocity prediction from speckle dynamic maps is not only related to the spatial pixel value of a single frame, but also related to the change of the pixel value at the fixed position between frames. The larger the change of pixel value, the faster velocity, as show in Fig. 4, the higher velocity has greater amplitude and frequency.

In the above data set, dynamic maps with speed of 0.18 mm/s and 3.63 mm/s, a random pixel (such as the pixel at 16 columns and 100 rows) is selected as fixed point, as shown in Fig. 3(b). The waveform of the pixel value at this point changing with the frame (1–500 frames) is shown in Fig. 4.

Fig. 5 is a single frame speckle image with m rows and n columns. the pixel position is represented by two-dimensional coordinates (i, j), where i and j represent the row number and column number of the pixel position.

In time domain, for a fixed position pixel, the pixel value is a typical one-dimensional sequence in the time series; In spatial domain, for any number of frames f, the pixel value at (i, j) position is $p(i, j)f$, and the pixel data of the whole pixel matrix can be described as matrix V of

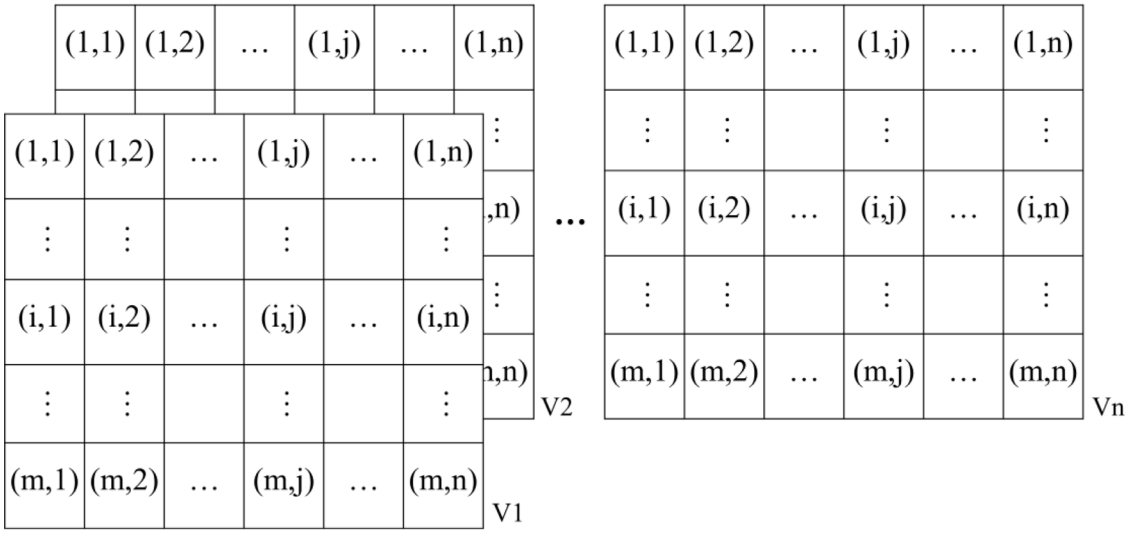

Fig. 6. spatio-temporal pixel distribution of speckle image (f = 1,2,3…).

$m \times n$:

$$V = \begin{bmatrix} p(1,1)_f & p(1,2)_f & \dots & p(1,n)_f \\ p(2.1)_f & p(2,2)_f & \dots & p(2,n)_f \\ \cdot & \cdot & \cdot & \cdot \\ \cdot & \cdot & \cdot & \cdot \\ \cdot & \cdot & \cdot & \cdot \\ p(m,1)_f & p(m,2)_f & \dots & p(m,n)_f \end{bmatrix} (f = 1,2,3\dots)$$

The elements of this speckle 3D pixel value matrix contain rich spatio-temporal feature information at a certain velocity v. The whole spatio-temporal sequence can be regarded as multiple frame movement, as shown in Fig. 6. Therefore, a spatio-temporal sequence consisting of speckle dynamic map pixel values representing different velocities can describe the velocity through the variation characteristics of array pixel values. The sequence of pixel values composed of n velocity speckle dynamic maps is$\{V1, V2,\dots, Vn\}$.

The pixel value matrix of each speckle dynamic map is a complete three-dimensional matrix. Therefore, in order to mine the spatio-temporal feature of the above matrix sequence on the premise of ensuring the integrity of spatio-temporal information, 3D-CNN is used as a prediction method in this paper to extract the overall features and organically complete the prediction.

3. The 3D-CNN model

Based on the above analysis, to ensure the integrity of speckle pixel information, this paper uses the speckle 3D pixel value matrix as the model input. At the same time, 3D-CNN is, for the first time, introduced to flow velocity prediction for improving LSCI imaging accuracy. In comparison to 2D-CNN, 3D-CNN adds time dimension information [27], enabling to extract and identify features and correlation information between consecutive frames. Therefore, the 3D convolution kernel of the model can directly study the global features of the speckle pixel value matrix.

The blood flow velocity prediction model based on this experimental data is mainly composed of the following parts, as shown in the upper part of Fig. 7. The prediction idea is divided into three parts: First, according to the pixel values of the speckle dynamic maps which have spatial characteristics of a single frame and the temporal characteristics between multiple frames, the three-dimensional matrix of the speckle pixel values is used as the input data; Second, the gradient images are extracted and dimensionally changed through the 3D-CNN network composed of convolution, pooling and full connection, and the predicted blood flow velocity represented by each speckle dynamic map is obtained respectively; Finally, the predicted blood flow velocities of the speckle dynamic maps is output.

Since the speckle 3D pixel value matrixes are spatio-temporal-simultaneous, in order to better mine the relationship between the characteristics of these pixel values and the velocity, this paper extracted the primary and secondary gradients of the speckle 3D pixel value matrix, obtained the gradient image, then analyzed and processes it through the 3D-CNN network. The gradient direction is the fastest changing direction of the function, and it is easier to find the maximum value of the function along the gradient vector direction; On the contrary, along the opposite direction of the gradient vector, the gradient decreases the fastest, and it is easier to find the minimum value of the function, which corresponds to finding the minimum value of the loss function in the 3D-CNN model to make the prediction result as close to the real result as possible. Taking the x direction as an example, the gradient extraction process is as follows:

$$f'(x) = \lim_{h \to 0} f(x+h) - f(x-h)/2h \tag{1}$$

Speckle 3D pixel value matrix is a three-dimensional image composed of numerous discrete pixel values, that is, it needs to be discrete according to pixels. Therefore, the minimum h in the central difference function of Eq. (1) is 1 pixel.

The first and second derivatives of the image in the x direction are shown in Eqs. (2) and (3):

$$\partial f/\partial x = f(x+1) - f(x) \tag{2}$$

$$\partial^2 f/\partial x^2 = f(x+1, y) + f(x-1, y) - 2f(x, y) \tag{3}$$

In gradient extraction, the first-order and second-order derivatives of a point in a certain direction are subtracted from the original image to obtain the gradient image in the corresponding direction.

In CNN, the area covered by the convolution kernel named the receptive field, which is also the size of the area mapped on the input picture by the pixels on the feature map output from each layer of the network. Therefore, there is a strong spatio-temporal correlation between the pixel values located in the same receptive field. Starting from the input layer, 3D-CNN uses 3D convolution kernel to extract the spatio-temporal information in the pixel matrix, after summarizing the features, it forms a new feature map and transmits it to the next layer for further processing.

As shown in the lower left part of Fig. 7, assuming that the size of the input speckle image is $10 \times 10 \times 10$ (the length and width of each speckle image are 10, which means 100 pixels included; the time dimension is

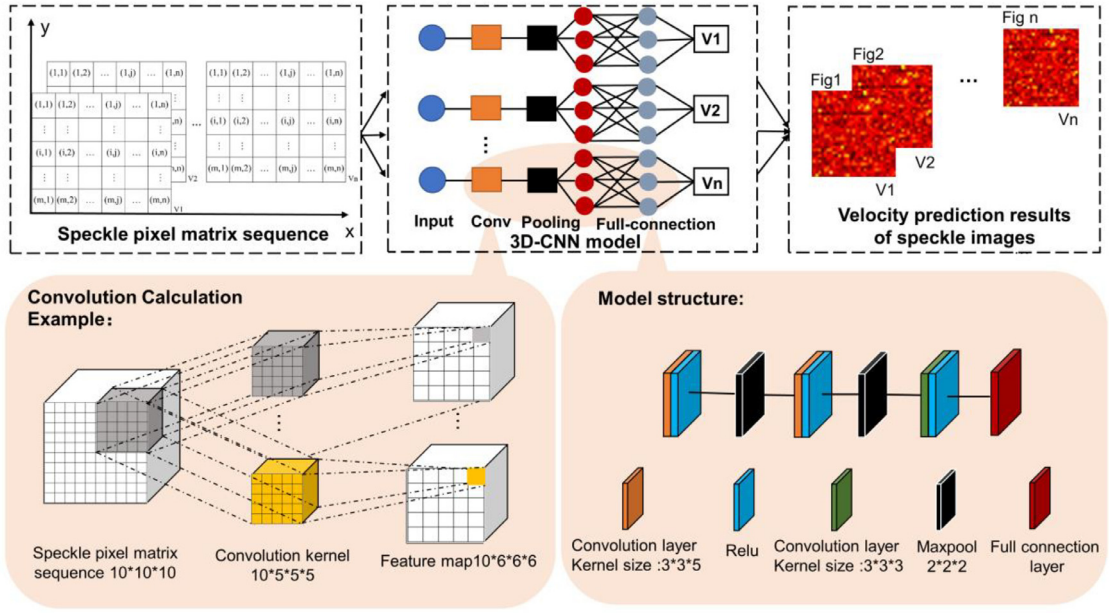

Fig. 7. LSCI blood flow velocity prediction model.

10, means 10 frames), the convolution layer of 3D-CNN has 10 convolution kernels, and the size of each convolution kernel is $5 \times 5 \times 5$, then the convolution will generate a feature map with the size of $6 \times 6 \times 6$ (10–5 + 1), and the number is 10. In such a decreasing way, 3D-CNN uses convolution kernel to obtain spatio-temporal feature information in speckle pixel values. The convolution process is shown in Eq. (4) [28].

$$V_{ij}^{xyz} = f\left(b_{ij} + \sum \sum_{p=0}^{P_i-1} \sum_{q=0}^{Q_i-1} \sum_{r=0}^{R_i-1} W_{ijk}^{pqr} U_{(i-1)k}^{(x+p)(y+q)(z+r)}\right) \tag{4}$$

Where the left side of the equal sign represents the output value of the i_{th} characteristic sequence of points (x, y, z) of the i_{th} layer; f is the activation function; b_{ij} is the additional deviation; k is the number of characteristic maps of layer $(i-1)$; P,Q and R respectively represent the spatial digits of the three-dimensional convolution kernel; W_{ijk}^{pqr} is the convolution kernel weight of the k_{th} feature map of the previous layer.

The middle part of Fig. 7 shows the process of 3D-CNN using 3D convolution kernel to extract spatio-temporal features related to flow velocity from speckle pixel matrix, that is, each network layer continues to extract features based on the feature map output from the previous layer, continuously capture feature information, and finally match the corresponding flow velocity label after dimensionality reduction in the full connection layer to complete velocity prediction.

3.1. CNN-LSCI setup

From the perspective of time series, the speckle dynamic map is multi-frame motion, that is, the intensity changes of a single pixel strongly depend on the velocity of the dynamic map. From the perspective of spatial sequence, each speckle image contains a lot of speckle pixel value information. Therefore, the accuracy of speed prediction depends on obtaining abundant time-series information. At the same time, it is also necessary to make full use of the pixel value information of a single frame and combine the two kinds of information for velocity prediction. The procedures of setting up the 3D-CNN model are divided into two steps:

Step 1: Preprocess the experimental data of the rotating scattering plate used to simulate blood flow. Intercept the appropriate image size and frame number, pack them as the input data, and use the corresponding speed as the label, that is, the training target.

Step 2: A 3D-CNN model was trained by using the experimental data of the rotating scattering plate phantom. The model was applied to predict the corresponding velocities of the speckle dynamic maps of 10 rotating scattering plates speckle images, and compared with the results of the single exposure LSCI and MELSIC to verify the accuracy of CNN-LSCI model.

3.2. Data preprocessing

In the training process, two factors need to be weighed when determining the input time series f, that is, the difficulty of model training and the integrity of prediction information. Too small f will lead to insufficient information contained in the time series to support the model training. On the contrary, too large f will increase the difficulty of model training and affect the model convergence and parameter optimization. Therefore, this paper sets the time series with a length of 15 frames as the most appropriate, and the square space size of 32×32 is more suitable for feature extraction of convolution kernel, that is, the rectangular parallelepiped speckle image with a size of $32 \times 32 \times 15$ is used as the model input.

In order to obtain the appropriate data volume, the radius is selected by sliding window to enhance the data. A 32×32 square sliding window is used to slide from the 32nd pixel to the 320th pixel from top to bottom to change the radius size in 32 steps, as show in Fig. 3(c). This method can obtain 9 radii, 1024 frames of data are collected for each radius, and 10 angular velocities are set in total. Therefore, 92,160 ($9 \times 1024 \times 10$) data can be obtained for training. The radius length represented by each pixel is 0.037 mm, and the number of pixels corresponding to the radius varies from 48 to 304. Therefore, the radius is approximately from 2 mm to 12 mm, corresponding to the angular velocity distribution from 0.05 rad/s to 1 rad/s. So that, the corresponding velocity range is approximately 0.1 mm/s to 12 mm/s, which has a wide range and continuity, and is of significant for model training.

The above 92,160 experimental data of the rotating scattering plate is, then, divided as a data set. The division ratio of Training Set vs Verification Set vs Test Set is 7:1:2.

Table 2
3D-CNN Parameter configuration.

Layer	Type	Configuration
—	Input	Size:32 × 32 × 15
1	C1	Kernel size:3 × 3 × 5;Activation function:Relu;Output dimensions:32
2	P2	Pooling size:2 × 2 × 2
3	C3	Kernel size:3 × 3 × 5;Activation function:ReLU;Output dimensions:64
4	P4	Pooling size:2 × 2 × 2
5	C5	Kernel size:3 × 3 × 3;Activation function:ReLU;Output dimensions:128
6	F6	Input dimensions:128;Output dimensions:1

Table 3
Parameters of 3D-CNN prediction process.

Layer	Input	C1	P2	C3	P4	C5	F6
Kernel size(F)	—	3 × 3 × 5	2 × 2 × 2	3 × 3 × 5	2 × 2 × 2	3 × 3 × 3	—
Padding(P)	—	1 × 1 × 1	1 × 1 × 1	1 × 1 × 1	1 × 1 × 1	1 × 1 × 1	—
Stride(S)	—	1	2	1	2	1	—
Feature map size	32×32×15	32×32×13	17×17×7	17×17×5	9 × 9× 3	9 × 9× 3	1

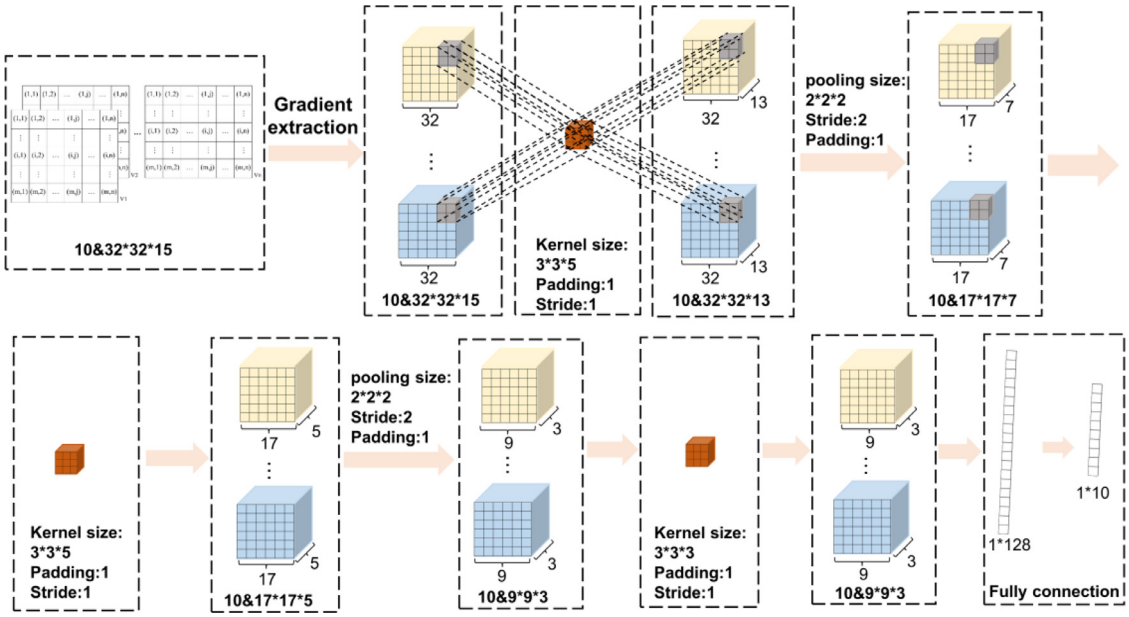

Fig. 8. 3D-CNN prediction process.

3.3. CNN-LSCI model

The 3D-CNN network based on Pytorch proposed in this paper has six layers, the first layer is convolution layer C1, which directly accepts the input speckle data and uses a convolution kernel of 3 × 3 × 5; The second layer is the maximum pool layer P2, and the pool core is 2 × 2 × 2; The third layer is the convolution layer C3, using a convolution kernel of 3 × 3 × 5; The fourth layer is the maximum pooling layer P4, the pooling core is 2 × 2 × 2, and the fifth layer is the convolution layer C5, using a convolution core of 3 × 3 × 3; The sixth layer is the fully connected layer F6, which reconstructs the 3D characteristic map output from C5 into a single velocity data, with an input dimension of 128 and an output dimension of 1. The convolution layer activation function of this model is Relu function. The optimizer uses Adam to accelerate the convergence speed. The batch size is 32, the initial learning rate is 0.001, and the loss function is MSE function. It is used for model training and testing of 1000 iterations. The parameter configuration of 3D-CNN is show in Table 2 and the lower right part of Fig. 7. MSE and MAPE are used as evaluation indicators, and the formula is as follows:

$$MSE = \sum_{i=1}^{m} \left(y_i - \hat{y}_i\right)^2 / m \tag{5}$$

$$MAPE = 100\% \times \sum_{i=1}^{n} \left|\left(y_i - \hat{y}_i\right)/y_i\right| / n \tag{6}$$

3.4. Model evaluation

In order to test the prediction performance of this 3D-CNN model, we used the speckle image when the sliding window moved to the position 97–128 as the prediction data, as shown in Fig. 3(d). This position is basically in the middle of the whole speckle, and the corresponding radius is about (97 + 16) × 0.037 = 4.2 mm. The linear velocity under this radius varies moderately with the angular velocity and the overall coverage is wide, which is 4.2 × 0.047 ~ 4.2 × 0.952 = 0.2 mm/s ~ 4.0 mm/s, a total of 10 velocities, as shown in Table 4. It covers the typical range of human blood flow velocity [29].

The prediction process of 3D-CNN model for each dynamic map is shown in Fig. 8. The size of each feature map can be obtained from Eq. (7), and the parameters are shown in Table 3.

$$N = (W - F + 2P)/S + 1 \tag{7}$$

Where N is the output size, W is the input size, F is the convolution kernel size, P is the padding size, and S is the stride.

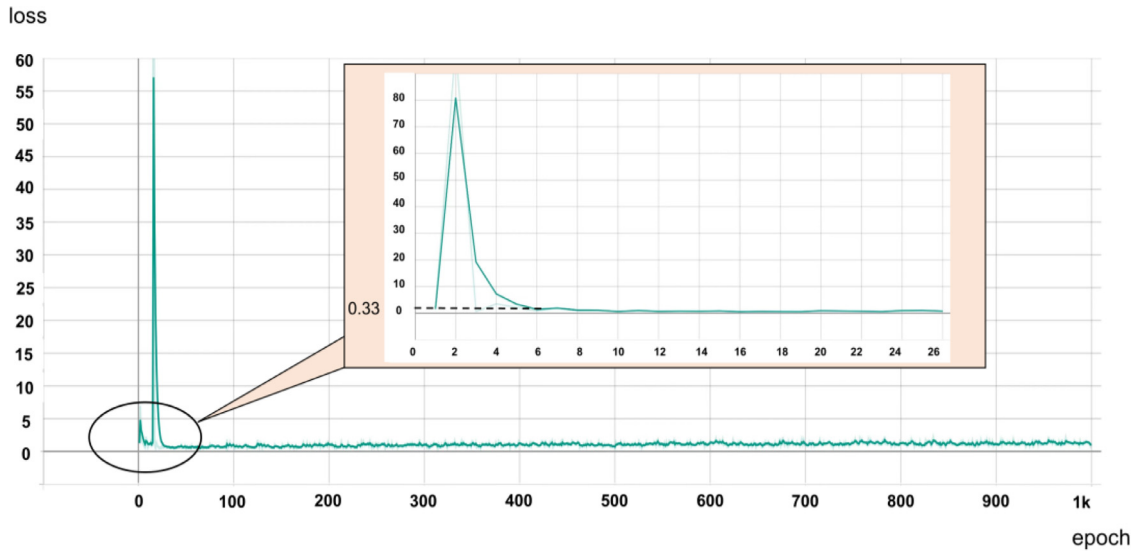

Fig. 9. 3D-CNN training monitoring curve, the enlarged window shows the convergence results of 3D-CNN after early stopping.

Table 4
Actual velocities and CNN prediction velocities of LSCI image.

Num	1	2	3	4	5	6	7	8	9	10
Actual velocity (mm/s)	0.20	0.44	0.88	1.33	1.78	2.22	2.67	3.11	3.56	4.00
Predicted velocity (mm/s)	0.25	0.54	0.96	1.41	1.76	2.17	2.56	2.91	3.45	3.85

First, the speckle 3D pixel value matrix with a size of $32 \times 32 \times 15$ are input into the 3D-CNN model and gradient extraction is performed; Second, the convolution kernel of $3 \times 3 \times 5$ is used for feature extraction, and the filling is set to 1 and the step size is set to 1 to obtain a feature image of $32 \times 32 \times 13$; Third, the maximum value pooling is performed. The pooled kernel size is $2 \times 2 \times 2$, the step size is 2, and the filling is set to 1 to obtain a characteristic image of $17 \times 17 \times 7$; Forth, performing the same convolution and pooling again; Fifth, the convolution kernel of $3 \times 3 \times 3$ is used for feature extraction, and the filling is set to 1 along with the step size 1 to obtain a feature image of $9 \times 9 \times 3$.

Finally, a one-dimensional data is obtained by reducing the dimension of the feature image through the full connection layer, that is, the predicted value of the velocity.

4. Results

The result of 3D-CNN trained with experimental data of rotating scattering plate is: MSE = 0.33, MAPE = 0.34. The monitoring curve of loss during training is shown in Fig. 9. It can be seen that the model has converged within 50 epochs. Therefore, the enlarged window in Fig. 9 shows the result after adding the early stop algorithm due to fast convergence, the epoch stays at 26, Loss still converges to 0.33. Each test data is a 15-frame speckle image with a fixed exposure time of 10.4 ms.

The prediction results of the 3D-CNN model for the ten velocities (0.2–4 mm/s, step is 0.445 mm/s) covering the typical blood flow velocity range of human body (0-2 mm/s) are shown in Table 4. The comparison curve between the predicted velocities and the actual velocities are shown in Fig. 10.

The correlation coefficient is used for evaluation, and the result is $R = 0.98$, which is highly correlated. The formula is as follows:

$$\rho XY = Cov(X, Y) / \sqrt{[D(X)][D(Y)]} \tag{8}$$

It can be seen from Fig. 10 that there is a small error between the predicted velocity and the actual velocity. The smallest error is presented when the velocity is 1.78 mm/s and 2.22 mm/s. The correlation with the actual speed reaches 0.98.

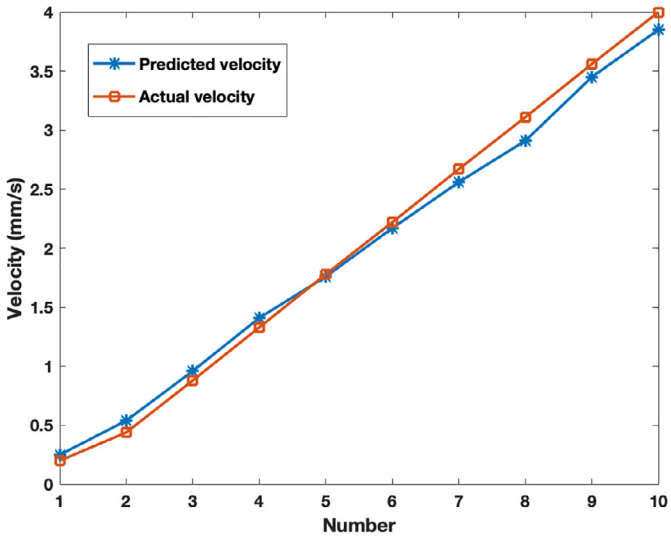

Fig. 10. Comparison curve between 3D-CNN predicted velocity and actual velocity.

In order to further measure the prediction performance of 3D-CNN, we used the traditional single exposure LSCI and the MELSCI to calculate the velocities of the above 10 speckle dynamic maps and compared with the prediction results of CNN-LSCI. LSCI obtained the velocity by calculating the contrast of a single frame image. MELSCI used the original speckle image of 1024 frames to obtain the contrast of multiple exposure times (0.064 ms, 0.128 ms, 0.256 ms, 0.512 ms, 1.024 ms, 2.048 ms, 4.096 ms, 8.192 ms, 16.384 ms, 32.768 ms, 65.536 ms), and

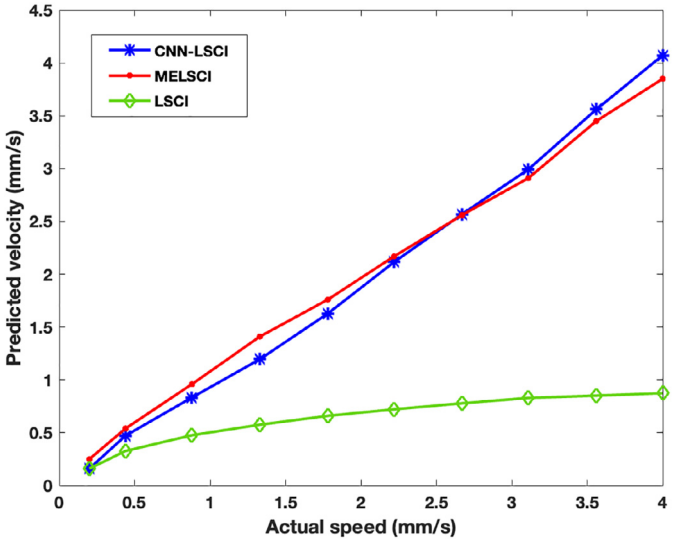

Fig. 11. Ten velocities of LSCI, MELSCI and CNN-LSCI.

then fitted the velocities by the trust-region-reactive algorithm. It can be seen that the results of traditional LSCI are greatly underestimated and seriously deviate from the actual velocity (as shown in Fig. 11). MELSCI shows high measurement accuracy, and it is almost linear with the actual velocity. However, the fitting process was performed offline. CNN-LSCI realizes a linear measurement within less time consumption in comparison to MELSCI.

5. Conclusion and discussion

This paper proposes a laser speckle-based velocity prediction method using machine learning. Three-dimensional convolutional neural network (3D-CNN) is, for the first time to our knowledge, applied to LSCI for velocity prediction. The spatio-temporal features of 15-frame speckle images are extracted by 3D convolution kernel to setup the CNN-LSCI model. This model is trained and evaluated by using experimental data of rotating diffuser. The accuracy of the CNN-LSCI is demonstrated at ten phantom velocities (0.2-4 mm/s) covering the typical blood flow velocity range.

This study compared the performance among CNN-LSCI, traditional single exposure LSCI and MELSCI. The results show that CNN-LSCI can predict phantom velocities in high accuracy that is comparable to MELSCI. Nevertheless, fixed exposure time and less used frames make it implemented easier as single exposure LSCI.

In terms of data set, there is also a scheme to use Monte Carlo simulation data for AI modelling. However, the simulation data rarely take account the noise introduced by optics and imaging system. The data used in this study is captured by the target system in practice. Therefore, both instrument noise and optical noise introduced during imaging can be eliminated by the “black box”. As a result, the model is more robust and accurate.

In this study, 15 frames are selected as the best frame number for feeding the model. This number is AI structure dependent and verifies with the configuration parameters, such as convolution kernel size, convolution layers, etc. In the rotating diffuser experiment, 1024 continues frames at each spinning speed were captured. This forms a relatively huge dataset (more than 10 million data), providing flexibility of exploring different AI structures or configurations.

Other models such as RNN (Recurrent Neural Network) and ANN (Artificial Neural Network) have demonstrated great advantages in extracting features from time series [30,31]. However, these methods can only extract the time features represented by a single pixel between speckle motion picture frames. In fact, the data bundle based on 15 frames contains both temporally interreacted pixels and spatially interreacted pixels. In light of the 3D convolution, the 3D-CNN employed in this paper can extract both of the spatial and temporal features of the input speckle dynamic map, making full use of the pixel information. Consequently, more comprehensive relations between the speckle image and the corresponding velocities have been mined.

It can be seen from Fig. 10, overestimations happened at low speed. However, the velocity is slightly underestimated when the speed is high. This means the CNN-LSCI model is relatively less sensitive to small velocity and high velocity. To overcome this, the model can be trained in wider velocity range and operated at narrower range. The sensitivity could also be increased by using the data with multiple exposure times which covers larger detectable velocities. Different configurations and other AI models are also worth to explore further to make any improvements.

It is worth noting that the CNN-LSCI model is only verified with phantom data. A few steps are demanded to make it applicable to blood flow imaging.

1) Reconstructing the CNN-LSCI model with suitable laser source. In this study, the wavelength of the laser is 532 nm which is not suitable for blood flow measurement. Replacement of a red or near infrared laser source (650 nm ~ 850 nm) will be taken in the future.
2) Utilization of cross polarizers. For the rotating diffuser used in this study, a large percentage of light that collected by the system is scattered from the static diffuser. As a result, the spatial variances include both dynamic scattering and the light scattered from the stationary surface, resulting large bias (variations) when constructing the CNN-LSCI model. For the human tissue where smaller percentage of static scattering present, a cross polarizer could be applied to reduce the surface reflections (light scattered from static scattering). This could further improve the CNN-LSCI model in terms of immunity to surface reflections (optical noise).
3) Performing transfer learning to finalize the CNN-LSCI model for in vivo measurement. In consideration of the differences between the phantom and human tissues in terms of optical paths and light transfer properties, the performance of the CNN-LSCI model may verify when applied to measure blood flow. This could be eliminated by performing transfer training with golden standard reference (e.g. laser Doppler blood flowmetry).

Details will be presented in our future works and publications.

Author statement

Xiaoqi Hao: Software, Data curation, Formal analysis, Visualization, Writing – Original Draft, Writing – Review & Editing

Shuicai Wu: Supervision, Resources

Lan Lin: Data analysis, Resources

Yixiong Chen: Data analysis, Resources, Conceptualization, Methodology

Stephen P. Morgan: Conceptualization, Methodology, Writing – Review & Editing

Shen Sun: Conceptualization, Methodology, Resources, Writing – Review & Editing, Supervision, Project administration, Funding acquisition

Compliance with ethical standards

All authors certify that they have no affiliations with or involvement in any organization or entity with any financial interest or non-financial interest in the subject matter or materials discussed in this manuscript.

Declaration of Competing Interest

The authors declare that they have no conflict of interest.

Data availability

Data will be made available on request.

Acknowledgments

The authors acknowledge the the program of China Scholarship Council (CXXM20210004).

References

[1] Potapova EV, Seryogina ES, Dremin VV, Stavtsev DD, Kozlov IO, Zherebtsov EA, Mamoshin AV, Ivanov YuV, Dunaev AV. Laser speckle contrast imaging of blood microcirculation in pancreatic tissues during laparoscopic interventions. Quant Electr 2020;50(1):33–40. doi:10.1070/QEL17207.
[2] Sia W, Lee C, Wang T, Chen W, Chang F, Tsai M. Investigation of laser-indued thermal effect with laser speckle contrast imaging. In: Proc. SPIE. 119251 M; 2021.
[3] Feng X, Yu Y, Zou D, Jin Z, Zhou C, Liu G, Fujimoto JG, Li C, Lu Y, Ren Q. Functional imaging of human retina using integrated multispectral and laser speckle contrast imaging. J Biophotonics 2021;15(2):e202100285. doi:10.1002/jbio.202100285.
[4] Lu Y, Zhou H, Zhou X, Chen Y, Wang R. Correlation between laser speckle flowgraphy and oct-derived retinal and choroidal metrics in healthy human eye. Transl Vis Sci Technol 2022;11(6):15. doi:10.1167/tvst.11.6.15.
[5] Mennes OA, Netten JJ, Baal JG, Steenbergen W. Assessment of microcirculation in the diabetic foot with laser speckle contrast imaging. Physiol Meas 2019;40(1):065002. doi:10.1088/1361-6579/ab2058.
[6] Mennes OA, Netten JJ, Baal JG, Slart RHJA, Steenbergen W. The association between foot and ulcer microcirculation measured with laser speckle contrast imaging and healing of diabetic foot ulcers. J Clin Med 2021;10(17):3844. doi:10.3390/jcm10173844.
[7] Couturier A, Bouvet R, Cracowski J, Roustit M. Reproducibility of high-resolution laser speckle contrast imaging approaches to assess cutaneous microcirculation for wound healing monitoring in mice. Microvasc Res 2022;141:104319. doi:10.1016/j.mvr.2022.104319.
[8] Philimon SP, Huong AKC. Laser speckle Integrated Multispectral Imaging System for In-Vivo assessment of diabetic foot ucler healing: a clinical study. IEEE Access 2021;9:23726–36. doi:10.1109/ACCESS.2021.3055221.
[9] Dyachenkotimoshina PA, Bashkatov AN, Alexandrov DA, Kochubey VI, Tuchin VV. Laser speckle contrast imaging for monitoring of acute pancreatitis at ischemia-reperfusion injury of thepancreas in rats. J Innov Optical Health Sci 2022;15:2242002. doi:10.1142/S1793545822420020.
[10] Im J, Kong TH, Choi JS, Seo YJ, Choi EC, Jung B, Kim J. Non-invasive postoperative monitoring of pedicled rat skin flap using laser speckle contrast imaging. Microvasc Res 2020;132:10405. doi:10.1016/j.mvr.2020.104050.
[11] Tamoiunas M, Vaitkien S, Miktait N, Galalyt D, Daugelaviius R. Assessment of Candida albicans biofilm growth by laser speckle contrast imaging. Third International Conference Biophotonics. 11585, 1158509; 2020. doi:101117/122582216.
[12] Liu C, Kilic K, Erdenerr SE, Boas DA, Postnov DD. Choosing a model for laser speckle contrast imaging. Biomedical Optics Express 2021;12(6):3571–83. doi:10.1364/BOE.426521.
[13] Kondász B, Hopp B, Smausz T. Mixed scattering as a problem in laser speckle contrast analysis. Appl Opt 2021;60(22):6593–9. doi:10.1364/AO.428785.
[14] Sang X, Li D, Chen B. A new simulation method for laser speckle imaging to investigate hemodynamics. In: 12th International Conference on Computational Heat, Mass and Momentum Transfer, 128; 2019. p. 02001. doi:10.1051/e3sconf/201912802001.
[15] Hu XB, Dong MX, Zhu ZH, Gao W, Rosales-Guzman C. Does the structure of light influence the speckle size? Sci Rep 2019;10:199. doi:10.1038/s41598-019-56964-0.
[16] Perez-Corona CE, Peregrina-Barreto H, Ramirez-San-Juan J. Space-directional approach to improve blood vessel visualization and temporal resolution in laser speckle contrast imaging. J Biomed Opt 2019;25(3):032009. doi:10.1117/1.JBO.25.3.032009.
[17] Guilbert J, Desjardins M. Movement correction method for laser speckle contrast imaging of cerebral blood flow in cranial windows in rodents. J Biophotonics 2022;15(1):e202100218. doi:10.1002/jbio.202100218.
[18] Parthasarathy AB, Tom WJ, Gopal A, Zhang X, Dunn AK. Robust flow measurement with multi-exposure speckle imaging. Opt Express 2008;16(3):1975–89. doi:10.1364/oe.16.001975.
[19] Hultman M, Fredriksson I, Larsson M, Alvandpour A, Stromberg T. A 15.6 frames per second 1-megapixel multiple exposure laser speckle contrast imaging setup. J Biophotonics 2018;11(2):e201700069. doi:10.1002/jbio.201700069.
[20] Y. Shimada, K. Takada, H.S. Nam, K. Miyazaki, K. Yasutomi, S. Kawahito, C. Crouzet, B. Choi, G.T. Kennedy, A.J. Durkin, K. Kagawa, 2022. A 2x2-aperture 4-tap multimodal tissue imager for multi-band SFDI and MELSCI. SPIE BiOS. 11951, 1195107. doi:10.1117/12.2608397.
[21] F. Lopez-Tiro, H. Peregrina-Barreto, J. Rangle-Magdaleno, J.C. Ramirez-San-Juan, 2021. Localization of blood vessels in in-vitro LSCI images with K-means. I2MTC. 20780194. doi:10.13140/RG.2.2.10286.02881/1.
[22] Cheng W, Lu J, Zhu X, Hong J, Liu X, Li M, Li P. Dilated residual learning with skip connections for real-time denoising of laser speckle imaging of blood flow in a log-transformed domain. IEEE Trans Med Imaging 2020;39(5):1582–93. doi:10.1109/TMI.2019.2953626.
[23] I. Stebakov, E. Kornaeve, D. Stavtsev, E. Potapova, V. Dremin, Laser speckle contrast imaging and machine learning in application to physiological fluids flow rate recognition. Vibroengnieering Procedia. 38(2021)50–55. doi:10.21595/vp.2021.22013.
[24] Kornaeva EP, Stebakov IN, Kornaev AV, Dremin VV, Popov SG, Vinokurov AY. A method to measure non-Newtonian fluids viscosity using inertial viscometer with a computer vision system. Int J Mech Sci 2022;242(15):107967. doi:10.1016/j.ijmecsci.2022.107967.
[25] Fredriksson I, Hultman M, Strmberg T, Larsson M. Machine learning in multiexposure laser speckle contrast imaging can replace conventional lasre Doppler flowmetry. J Biomed Opt 2019;24(1):016001. doi:10.1117/1.JBO.24.1.016001.
[26] Sun S. Laser doppler imaging and laser speckle contrast imaging for blood flow measurement. University of Nottingham; 2013 https://ethos.bl.uk/OrderDetails.do?uin=uk.bl.ethos.604304.
[27] Zhao X, Wei H, Wei H, Wang H, Zhu T, Zhang K. 3D-CNN-based feature extraction of ground-based cloud images for direct normal irradiance prediction. Sol Ergy 2019;181:510–18. doi:10.1016/j.solener.2019.01.096.
[28] Ji S, Xu W, Yang M, Yu K. 3D Convolutional Neural Networks for human action recognition. IEEE Trans Pattern Anal Mach Intell 2013;35(1):221–31. doi:10.1109/TPAMI.2012.59.
[29] Sun S, Hayes-Gill BR, He D, Zhu Y, Huynh NT, Morgan SP. Comparision of laser Doppler and laser speckle contrast imaging using a concurrent processing system. Opt Laser Eng 2016;83:1–9. doi:10.1016/j.optlaseng.2016.02.021.
[30] Hochreiter S, Schmidhuber J. Long short-term memory. Neural Comput 1997;9(8):1735–80. doi:10.1162/neco.1997.9.8.1735.
[31] Zhang Y, Pan G, Chen B, Han J. Short-term wind speed predic-tion model based on GA-ANN improved by VMD. Renew Energy 2020;156:1373e88. doi:10.1016/j.renene.2019.12.047.

Xiaoqi Hao was born in Datong, Shanxi, China, in 1998. She received the B.S. degree in biomedical engineering from North University of China. She is now pursuing a master's degree in biomedical engineering from Biomedical Electronic Laboratory, Faculty of Environment and Life Science of Beijing University of Technology. Her research interests are in laser speckle contrast blood flow imaging.

Shuicai Wu is duty professor of biomedical engineering at Beijing University of Technology. He received PhD from Huazhong University of Science and Technology in 2000. He visited University of Warwick and University of Pittsburgh as academic visitor in 2008 and 2010 respectively. His-research interest is in biomedical electronics, biomedical signal processing and biomedical imaging processing.

Lan Lin was born in Wuhan, Hubei, China, in 1974. He received the B.S. degree in computer science from Wuhan University, the M.S. degree in biomedical engineering from Huazhong University of Science and Technology, and the Ph.D. degree in bioengineering from Arizona State University, USA, in 1996, 1999, and 2006, respectively. From 2006–2011, he visited the Department of Psychology in University of Arizona (USA) as a Postdoctoral Research Fellow. Since 2012, he works as an Associate Professor at Beijing University of Technology, China. His-professional research interest is in biomedical imaging.

Yixiong Chen is a project manager in Beijing Science and Technology Project Manager Management Corporation Ltd. Prior to that, He was a senior data scientist in IBM CIC China. He obtained his PhD in Applied Mathematics from King's College London in 2015. His-research interests include deep learning and quantum computing.

Stephen P. Morgan is Professor of Biomedical Engineering. Since 1992 he has investigated novel optical techniques for imaging and spectroscopy of tissue including laser Doppler blood flowmetry and ultrasound modulated optical tomography. Recently he has been developing novel medical devices based on optical fibre sensors.

Shen Sun is an assistant professor of Biomedical Engineering at Beijing University of Technology. He received his MSc and PhD degrees in Electronic Engineering from the University of Nottingham in 2009 and 2013 respectively. His-research focuses on full-field laser Doppler and laser speckle contrast blood flow imaging systems and development of medical devices and healthcare instruments.